bioRxiv preprint doi: https://doi.org/10.1101/2023.02.24.529908; this version posted February 25, 2023. The copyright holder for this preprint (which was not certified by peer review) is the author/funder, who has granted bioRxiv a license to display the preprint in perpetuity. It is made available under aCC-BY-ND 4.0 International license.

Outer hair cell receptor potentials reveal a local resonance in the mammalian cochlea

Andrei N Lukashkin[1,3,4,*], Ian J Russell[1], Oyuna Rybdylova[2,3,*]

[1]Sensory Neuroscience Research Group, School of Applied Science, University of Brighton, Brighton BN2 4GJ, United Kingdom

[2]Advanced Engineering Centre, School of Architecture, Technology and Engineering, University of Brighton, Brighton BN2 4GJ, United Kingdom

[3]These authors contributed equally

[4]Lead contact

*Correspondence: a.lukashkin@brighton.ac.uk (ANL), o.rybdylova@brighton.ac.uk (OR)

SUMMARY

Sensory hair cells, including the sensorimotor outer hair cells, which enable the sensitive, sharply tuned responses of the mammalian cochlea, are excited by radial shear between the organ of Corti and the overlying tectorial membrane. It is not currently possible to measure directly *in vivo* mechanical responses in the narrow cleft between the tectorial membrane and organ of Corti over a wide range of stimulus frequencies and intensities. The mechanical responses can, however, be derived by measuring hair cell receptor potentials. We demonstrate that the seemingly complex frequency and intensity dependent behaviour of outer hair cell receptor potentials could be qualitatively explained by a two-degrees of freedom system with a local cochlear partition and tectorial membrane resonances strongly coupled by the outer hair cell stereocilia. A local minimum in the receptor potential below the characteristic frequency is always observed at the tectorial membrane resonance frequency which, however, might shift with stimulus intensity.

Keywords: cochlea, cochlear amplifier, cochlear micromechanics, tectorial membrane, outer hair cell

INTRODUCTION

The mammalian cochlea is an impressively sensitive, sharp frequency analyser which works over a wide range of sound pressure levels (SPLs) exceeding six orders of magnitude (Robles and Ruggero, 2001). These features are associated with a process called the cochlear amplifier (Davis, 1983), which amplifies and sharpens cochlear responses to low-level sound

bioRxiv preprint doi: https://doi.org/10.1101/2023.02.24.529908; this version posted February 25, 2023. The copyright holder for this preprint (which was not certified by peer review) is the author/funder, who has granted bioRxiv a license to display the preprint in perpetuity. It is made available under aCC-BY-ND 4.0 International license.

stimulation but compresses them at mid to high stimulus levels. Cochlear amplification is observed only in healthy cochleae and it vanishes once cochlear function is compromised. The cellular basis of cochlear amplification is the sensory motile outer hair cells (OHCs) (Figure 1A) (Brownell et al., 1985; Liberman et al., 2002; Ashmore, 2008; Dallos, 2008; Mellado Lagarde et al., 2008). OHCs are mechanical effectors that change their length in response to changes in their transmembrane voltage (Ashmore 1987; Santos-Sacchi and Dilger, 1988). Length changes of the stiff OHCs can generate forces sufficient for minimising the damping of mechanical responses of cochlear structures surrounded by fluids (Gold, 1948; Lukashkin et al., 2007b; Dong and Olson, 2013). Three rows of OHCs are imbedded in the sensory organ of Corti (OoC) sitting on top of the extracellular basilar membrane (BM) that extends the length of the entire spiral cochlea (Figure 1A). The mechanoelectrical transducer (MET) channels of the OHCs are located close to the tips of the OHC sensory organelles, stereocilia, which form hair bundles that are imbedded in the extracellular tectorial membrane (TM) that covers the OoC, with the TM inner edge being elastically attached to the bony spiral limbus (Richardson et al., 2008). The OHC hair bundles provide a stiff mechanical link between the TM and the reticular lamina (RL) at the apical surface of the OoC. During radial shear between the TM and RL, the hair bundles are rotated about their attachment to the apical surface of the OHCs (Figure 1B), which leads to modulation of the MET current and generation of intra- and extracellular receptor potentials (RP) (Russell, 2008). RP generation results in changes in the OHC transmembrane voltage and associated OHC length changes. Hair bundles of the other type of sensory cell in the OoC, the inner hair cells (IHCs), which have rich afferent innervation and provide information to the brain, are free-standing and excited by flow of fluid entrained in the subtectorial space (STS, Figure 1A) during radial shear between the TM and RL (Sellick and Russell, 1980; Patuzzi and Yates, 1997; Nowotny and Gummer, 2006). The radial shear occurs during transversal BM vibrations (Figure 1B). The BM mechanical properties are graded and BM vibrations, which propagate as travelling waves (TWs) along the BM from the high-frequency base to low-frequency apex, peak at a frequency-specific, characteristic frequency (CF) place, where most of the TW energy is dissipated (Figure 1B) (von Békésy, 1960). Thus, the BM effectively functions as a frequency analyser separating constitutive frequency components of sounds in space and time. The TWs quickly die out at a cochlear place where the BM resonance frequency ω_{bm} (Figure 1B) is equal to the stimulus frequency (von Békésy, 1960). The BM is not stiff enough to support the TW beyond this point.

bioRxiv preprint doi: https://doi.org/10.1101/2023.02.24.529908; this version posted February 25, 2023. The copyright holder for this preprint (which was not certified by peer review) is the author/funder, who has granted bioRxiv a license to display the preprint in perpetuity. It is made available under aCC-BY-ND 4.0 International license.

The intricate structure of the cochlea (Figure 1A) appears to have evolved to enable fine-tuning of the OHCs responses and ensure optimal cochlear amplification to augment the stimulation of IHCs and, consequently, to provide adequate auditory information to the brain (Russell, 2008). Therefore, knowledge of the STS micromechanics is critical for understanding the workings of the cochlea. Current experimental methods for recording direct mechanical responses in the narrow cleft between the TM and RL do not have sufficient resolution *in vivo* to provide unambiguous data on the mechanics in this confined geometry over a wide range of stimulus frequencies and levels (Nowotny and Gummer, 2006). Fortunately, because the OHC hair bundles are embedded into the TM, and because the OHC RPs are generated due to radial shear between the TM and RL (Russell, 2008), measurement of the OHC RP can provide an insight into micromechanics of the STS. The current study demonstrates that the seemingly complex behaviour of the OHC RP recorded from a single OHC in the two-dimensional space of stimulus levels and frequencies at the cochlear base (Figure 2) (Kössl and Russell, 1992; Russell and Kössl, 1992; Levic et al., 2022) arises from a local resonance in every frequency place. A minimal mechanical arrangement, which still can explain the OHC RP behaviour, consists of a resonating BM and TM strongly coupled together via OHC stereocilia, with the TM resonance frequency located below the BM resonance frequency in every cochlear place (Allen, 1980; Zwislocki, 1980; Allen and Neely, 1992).

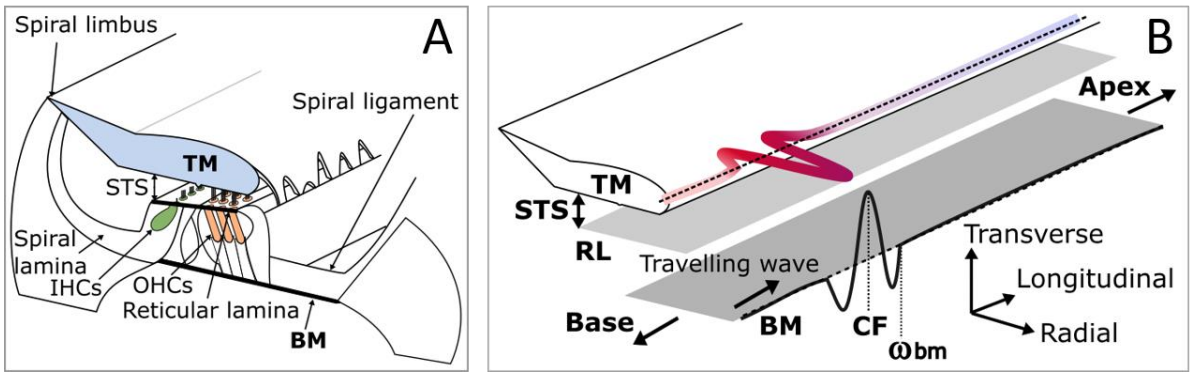

Figure 1. Schematics of the mammalian cochlea and the propagation of travelling wave along its length

BM, basilar membrane; TM, tectorial membrane; STS, subtectorial space; OHCs and IHCs are inner and outer hair cells, respectively; RL, reticular lamina; CF and ω_{bm} are the characteristic frequency place and BM resonance place for a given stimulus frequency, respectively.

(A) Schematic of the cochlear cross-section showing the relationship between the BM, the sensory OoC, sitting on top of the BM, and the TM overlaying the OoC. The TM is attached

bioRxiv preprint doi: https://doi.org/10.1101/2023.02.24.529908; this version posted February 25, 2023. The copyright holder for this preprint (which was not certified by peer review) is the author/funder, who has granted bioRxiv a license to display the preprint in perpetuity. It is made available under aCC-BY-ND 4.0 International license.

to the OHC sensory stereocilia and the spiral limbus but the IHC stereocilia are free standing and deflected by flow of fluid in the STS.

(B) TW propagation along the BM generates transversal movement of the BM (black wave). The TW slows down and its amplitude builds up, reaching a maximum at the CF, when the TW comes to the point where the BM resonance frequency, ω_{bm}, is the same as frequency of the sound stimulation. The TW does not propagate beyond the ω_{bm} place towards the cochlear apex because the stiffness of the BM is insufficient to support the TW. The transversal BM movement is transformed into radial shearing motion between the TM and RL (red wave), which, in turn, deflects stereocilia of sensory OHCs and IHCs. Modified from (Jones et al., 2013).

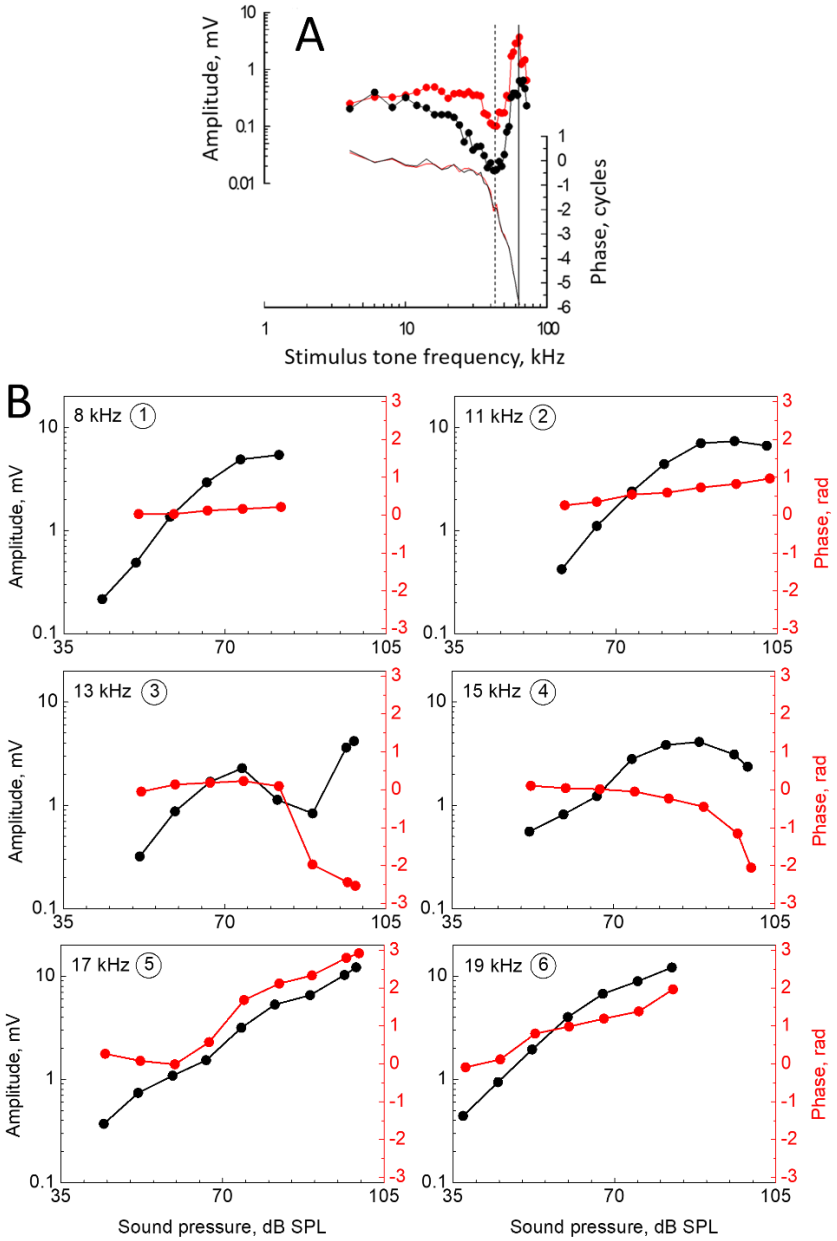

Figure 2. Outer hair cell receptor potentials recorded in mouse and guinea pig cochleae

(A) The 70 dB SPL isolevel frequency functions of the intracellular (black) and extracellular (red) receptor potentials recorded from the mouse cochlea. The data were compensated for

bioRxiv preprint doi: https://doi.org/10.1101/2023.02.24.529908; this version posted February 25, 2023. The copyright holder for this preprint (which was not certified by peer review) is the author/funder, who has granted bioRxiv a license to display the preprint in perpetuity. It is made available under aCC-BY-ND 4.0 International license.

recording electrode low-pass filter characteristics. Vertical solid lines indicate CF; dotted line indicate the frequency of amplitude minimum observed about half an octave below the CF. Phase was corrected for middle ear transfer characteristics (Dong et al., 2013), sound system, and recording electrode. Modified from (Levic et al., 2022).

(B) Amplitude (black) and phase (red) receptor potential level functions recorded extracellularly from a guinea pig OHC (CF is 18 kHz) at the frequencies indicated within each panel. The amplitude was compensated for the single-pole, low-pass filtering of the recording electrode (corner frequency is 3.5 kHz). Numbers in circles in each panel identify frequencies with relative positions as indicated in Figure 4C. Modified from (Kössl and Russell, 1992).

RESULTS

Linear Passive System

A minimal micromechanical model which still qualitatively reproduces the behaviour of the OHC RP is an Allen-Zwislocki-Neely type model (Allen, 1980; Zwislocki, 1980; Allen and Neely, 1992) in which the TM is able to resonate radially due to its elastic attachments to the OHC stereocilia and the spiral limbus (Figure 1A). For this model, each cross-section of the OoC with attached TM could be represented by a schematic shown in Figure 3A (see Allen (1980) for the equivalent of this schematic and a mechanical system with the TM-RL shear).

The system in Figure 3A is described by the following equations

$$M_{\mathrm{bm}}\frac{d^2X_{\mathrm{bm}}}{dt^2}+\eta_{\mathrm{bm}}\frac{dX_{\mathrm{bm}}}{dt}+K_{\mathrm{bm}}X_{\mathrm{bm}}-K_{\mathrm{c}}\Delta X=P(t); \tag{1}$$

$$M_{\mathrm{tm}}\frac{d^2X_{\mathrm{tm}}}{dt^2}+\eta_{\mathrm{tm}}\frac{dX_{\mathrm{tm}}}{dt}+K_{\mathrm{tm}}X_{\mathrm{tm}}+K_{\mathrm{c}}\Delta X=0, \tag{2}$$

where a harmonic external force $P(t)=P_a\sin(\omega t)$ of frequency ω and amplitude P_a is applied to the BM, and M_{bm} denotes the entire cochlear partition mass. $\Delta X=X_{\mathrm{tm}}-X_{\mathrm{bm}}$ is the relative displacement between the OoC and TM which excites the OHCs and, as a first approximation for small ΔX, could be used to make estimates of the OHC RP behaviour.

Substituting the characteristic parameters,

$$\omega_{\mathrm{bm}}=\sqrt{\frac{K_{\mathrm{bm}}}{M_{\mathrm{bm}}}},\quad \omega_{\mathrm{tm}}=\sqrt{\frac{K_{\mathrm{tm}}}{M_{\mathrm{tm}}}},\quad \omega_{\mathrm{c}}=\sqrt{\frac{K_{\mathrm{c}}}{M_{\mathrm{tm}}}},\quad \zeta_{\mathrm{bm}}=\sqrt{\frac{\eta_{\mathrm{bm}}}{M_{\mathrm{bm}}}},$$

$$\zeta_{\mathrm{tm}}=\sqrt{\frac{\eta_{\mathrm{tm}}}{M_{\mathrm{tm}}}}, \tag{3}$$

the system of equations (1, 2) may be rewritten as

bioRxiv preprint doi: https://doi.org/10.1101/2023.02.24.529908; this version posted February 25, 2023. The copyright holder for this preprint (which was not certified by peer review) is the author/funder, who has granted bioRxiv a license to display the preprint in perpetuity. It is made available under aCC-BY-ND 4.0 International license.

$$\frac{d^2X_{\mathrm{bm}}}{dt^2} + \zeta_{\mathrm{bm}}\frac{dX_{\mathrm{bm}}}{dt} + \omega_{\mathrm{bm}}^2 X_{\mathrm{bm}} - \omega_{\mathrm{c}}^2 \Delta X\left(\frac{M_{\mathrm{tm}}}{M_{\mathrm{bm}}}\right) = \frac{P(t)}{M_{\mathrm{bm}}}; \quad (4)$$

$$\frac{d^2X_{\mathrm{tm}}}{dt^2} + \zeta_{\mathrm{tm}}\frac{dX_{\mathrm{tm}}}{dt} + \omega_{\mathrm{tm}}^2 X_{\mathrm{tm}} + \omega_{\mathrm{c}}^2 \Delta X = 0. \quad (5)$$

We refer to ω_{bm} and ω_{tm} as the BM and TM resonance frequency, respectively, for the rest of the paper. For the chosen relationships between the model parameters, which are in line with those measured experimentally and used in other modelling studies (e.g. see Meaud and Grosh, 2014; Nankali et al., 2022), ΔX, i.e. relative displacement between M_{tm} and M_{bm}, demonstrates a local minimum at frequency ω_{tm} (Figure 3B). The minimum should result in a decrease in OHC excitation and, in turn, in a local minimum in the OHC RP observed about half an octave below the CF (Figure 2A). The minimum always occurs at the TM resonance frequency ω_{tm}, where the TM has a minimal impedance determined only by the viscous damping and, hence, minimal load on the OHC stereocilia, and its frequency position does not depend on the properties of the driven oscillator, i.e. the BM (see question 1 and an answer to it in the Supplemental Information for detailed derivation). The ΔX minimum becomes more pronounced with decreasing TM damping so that $\Delta X \to 0$ at frequency ω_{tm} when $\zeta_{\mathrm{tm}} \to 0$.

For the chosen model parameters, the minimum/antiresonance is not observed in the BM and TM responses for frequencies below ω_{bm} (Figure 3D). ΔX is stiffness dominated below the minimum (Figure 3C). ΔX becomes mass dominated at the amplitude minimum and a corresponding phase transition of π is observed (also see Equation S24 in the Supplemental Information). The corresponding phase transition is also observed near the minimum of the experimentally measured OHC RP (Figure 2A). ΔX becomes stiffness dominated close to the first normal mode of vibrations near ω_{bm} where local maximums of the BM and TM displacements (Figure 3D) and ΔX (Figure 3B) are observed, and where the ΔX phase angle returns to $-\pi/2$ (Figure 3C, Equation S24 in the Supplemental Information). It should be noted that the system of equations (4, 5) does not include the TW observed in the cochlea. Therefore, a large phase roll-off due to TW propagation (Figure 2A) is not observed in the model responses. The phase demonstrates only a transition up to 180 degrees (Figure 3C) for the mass-dominated responses between ω_{tm} and ω_{bm}, which is similar to that seen in figure 3 of Allen (1980). Also, because the model does not include TW, a sharp decline in the amplitude of the OHC RP above the CF (Figure 2A) is not observed in the model presented

bioRxiv preprint doi: https://doi.org/10.1101/2023.02.24.529908; this version posted February 25, 2023. The copyright holder for this preprint (which was not certified by peer review) is the author/funder, who has granted bioRxiv a license to display the preprint in perpetuity. It is made available under aCC-BY-ND 4.0 International license.

in Figure 3A. In the real cochlea, the TWs quickly die out at a cochlear place where the BM resonance frequency ω_{bm} is equal to the stimulus frequency (Figure 1B) and responses for frequencies above ω_{bm} cannot be recorded (von Békésy, 1960). This frequency region is indicated by horizontal grey arrows in Figures 3B, 4B. Hence, the second normal mode, which is shifted to frequencies well above ω_{bm} due to strong elastic coupling K_{c} between M_{tm} and M_{bm}, is not observed *in vivo* (see question 2 and an answer to it in the Supplemental Information for detailed derivation).

The role of the TM limbal attachment K_{tm} for OHC excitation was investigated experimentally by Lukashkin et al. (2012) and modelled by Meaud and Grosh (2014). Similar sensitivity and sharpness of BM tuning were found in wild-type mice and mutant mice with the TM detached from the spiral limbus. It was suggested that the elasticity of the TM attachment to the spiral limbus is not a crucial factor for exciting the OHCs near their CF, and that the OHCs must be excited by the inertial load provided by the TM mass at CF to effectively boost the mechanical responses of the cochlea. Indeed, while the ΔX minimum is not observed in model responses when $K_{\mathrm{tm}} = 0$ (Figure 3B, see question 3 and an answer to it in the Supplemental Information for detailed derivation), ΔX response is mass dominated and the phase angle is similar in both cases, $K_{\mathrm{tm}} > 0$ and $K_{\mathrm{tm}} = 0$, between ω_{tm} and ω_{bm} (Figure 3C). In the real cochlea, this frequency range corresponds to stimulus frequencies below the CF where the non-linear cochlear amplification gradually builds up (Nilsen and Russell, 1999; Robles and Ruggero, 2001; Zheng et al., 2007; Dong and Olson, 2013; Lee et al., 2016) and, thus, the ΔX phase angle and OHC excitation timing are optimal for cochlear amplification to occur. Therefore, similar ΔX excitation phase/timing for conditions $K_{\mathrm{tm}} = 0$ and $K_{\mathrm{tm}} > 0$ (Figure 3C), with $K_{\mathrm{tm}} = 0$ simulating mutants with the TM detached from the spiral limbus, supports the conclusion that the OHCs must be excited by the inertial load provided by the TM mass at CF to effectively boost the mechanical responses of the cochlea (Gummer et al., 1996; Lukashkin et al., 2010; Lukashkin et al., 2012; Meaud and Grosh, 2014; Nankali et al., 2022).

bioRxiv preprint doi: https://doi.org/10.1101/2023.02.24.529908; this version posted February 25, 2023. The copyright holder for this preprint (which was not certified by peer review) is the author/funder, who has granted bioRxiv a license to display the preprint in perpetuity. It is made available under aCC-BY-ND 4.0 International license.

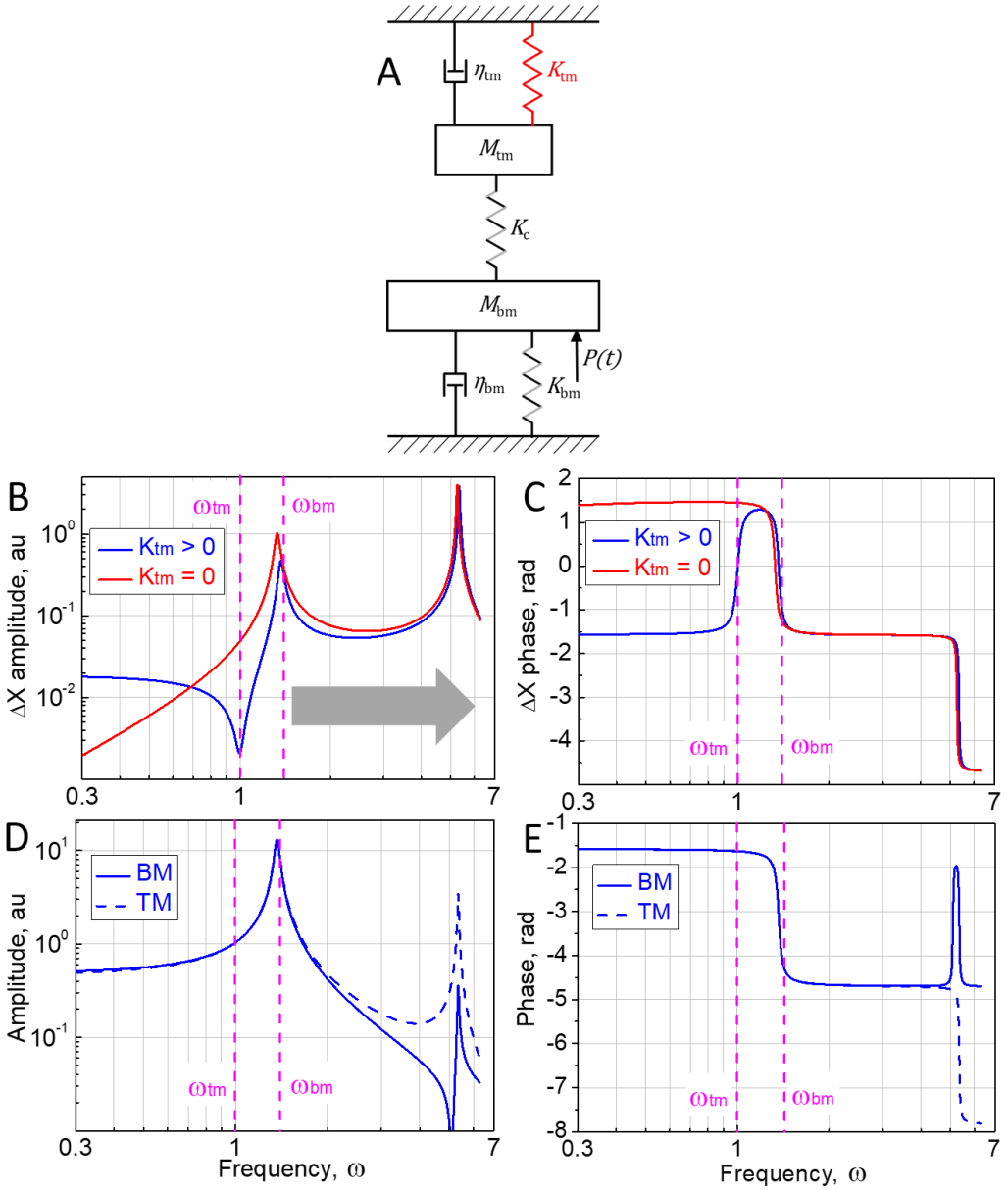

Figure 3. A schematic of cochlear cross-section with resonating tectorial membrane and its responses to harmonic excitation $P(t)$.

(A) A schematic showing the relationship between the mechanical elements in a cochlear cross-section. M_{tm} is the TM mass and M_{bm} denotes the entire cochlear partition mass; K_{tm} and K_{bm} are stiffnesses of the TM limbal attachment and BM stiffness respectively; K_c is elastic coupling between the TM and BM due to OHC stereocilia; η_{tm} and η_{bm} denote viscous damping of the TM and BM respectively. See the main text for more details.

(B) Amplitude and (C) phase responses for the relative displacement, ΔX, between the BM and TM.

(D) Amplitude and (E) phase responses of the BM and TM.

Vertical dashed magenta lines indicate ω_{tm} and ω_{bm} as defined by equation (3). Responses for the condition $K_{tm} = 0$ in panels (D) and (E) are not shown because at the given resolution they are superimposed with responses when $K_{tm} > 0$. Horizontal grey arrow in panel (B)

bioRxiv preprint doi: https://doi.org/10.1101/2023.02.24.529908; this version posted February 25, 2023. The copyright holder for this preprint (which was not certified by peer review) is the author/funder, who has granted bioRxiv a license to display the preprint in perpetuity. It is made available under aCC-BY-ND 4.0 International license.

indicates the frequency range where *in vivo* responses are not recorded because the BM TW does not propagate beyond the ω_{bm} place towards the cochlear apex (Figure 1B).

The following parameters were used to calculate the responses: $M_{\mathrm{tm}} = 1$, $M_{\mathrm{bm}} = 10$, $\omega_{\mathrm{tm}} = 1$, $\omega_{\mathrm{bm}} = 1.4$, $\omega_{\mathrm{c}} = 5$, $\zeta_{\mathrm{tm}} = \zeta_{\mathrm{bm}} = 0.05$, $P_{\mathrm{a}} = 10$.

Active Nonlinear System

The cochlear amplifier is introduced as a nonlinear damping (η_{n} in Figure 4A) which includes a level-independent positive damping and a level-dependent negative damping component (Gold, 1948; Elliott et al., 2015) demonstrated experimentally (Lukashkin et al., 2007b) so that

$$\zeta_{\mathrm{bm}} = \zeta_{\mathrm{bm}}^{+} + \zeta_{\mathrm{bm}}^{-} \tag{6}$$

and

$$\zeta_{\mathrm{tm}} = \zeta_{\mathrm{tm}}^{+} + \zeta_{\mathrm{tm}}^{-}, \tag{7}$$

where ζ^{+} and ζ^{-} are corresponding positive and negative components for the BM and TM damping. The cochlear amplifier emerges from the OHC length changes which are controlled by changes in the voltage across the OHC basolateral membrane (Ashmore 1987; Santos-Sacchi and Dilger, 1988). The transmembrane voltage changes, in turn, are generated by the MET current which is modulated when the OHC hair bundles are rotated about their attachment to the OHC apical cuticular plate due to the relative displacement between the OoC and TM (Russell, 2008). In this case, the OHC MET current is a function of ΔX. As a first approximation this function could be describes by a sigmoidal nonlinearity/Boltzmann function

$$N(\Delta X) = \frac{1}{1 + e^{a_1(x_1 - \Delta X)}}, \tag{8}$$

where $N(\Delta X)$ is the MET nonlinearity, a_1 sets the slope of the function, and x_1 is the position of maximum slope. Therefore, the negative damping for both the BM and TM could be defined as

$$\zeta^{-} = -\gamma \frac{dN(\Delta X)}{d\Delta X}, \tag{9}$$

where γ is the transfer ratio relating the change in the OHC receptor potential to resultant negative damping developed by the OHCs. To find numerical solutions of equations (4-9) in

bioRxiv preprint doi: https://doi.org/10.1101/2023.02.24.529908; this version posted February 25, 2023. The copyright holder for this preprint (which was not certified by peer review) is the author/funder, who has granted bioRxiv a license to display the preprint in perpetuity. It is made available under aCC-BY-ND 4.0 International license.

the time domain, γ was taken to be $\gamma = 4(\zeta^{+} - 0.0001)$ for both the BM and TM to ensure that the total damping is always positive.

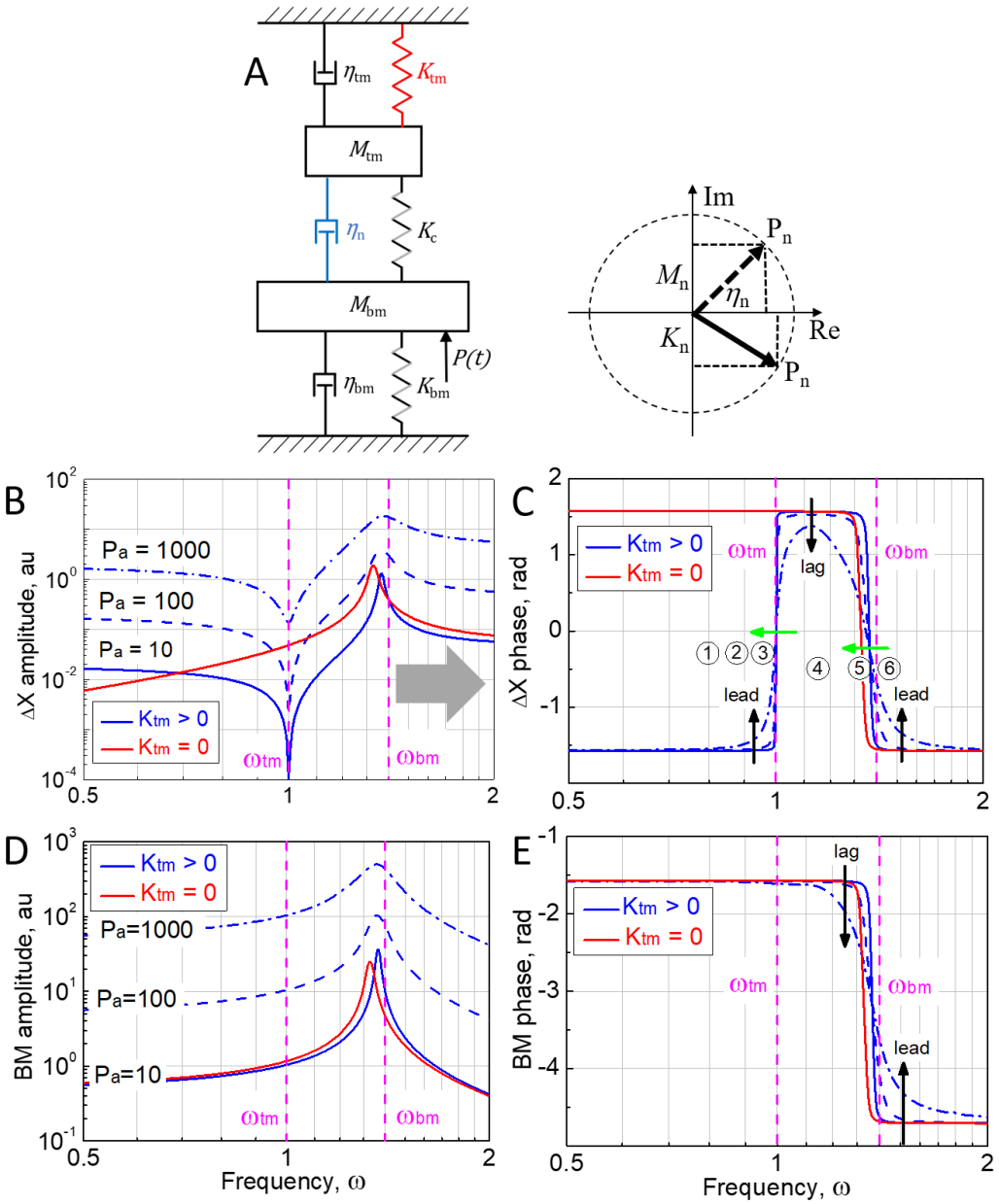

Figure 4. Response of the active model with nonlinear damping to harmonic excitation

(A) A schematic showing the relationship between the mechanical elements in a cochlear cross-section. M_{tm} is the TM mass and M_{bm} denotes the entire cochlear partition mass; K_{tm} and K_{bm} are stiffnesses of the TM limbal attachment and BM stiffness respectively; K_c is elastic coupling between the TM and BM due to the OHC stereocilia; η_{tm} and η_{bm} denote viscous damping of the TM and BM respectively; η_n is a nonlinear damping due to action of the OHCs. Only $P_a = 10$ response for $K_{tm} = 0$ is shown. Insert in (A) illustrates a situation when the nonlinear, level-dependent OHC force P_n is out of phase with the damping force η_n. In this case a nonlinear, level-dependent stiffness K_n (if P_n lags η_n) or mass M_n (if P_n leads η_n) associated with the OHC action is observed. See the main text for more details.

bioRxiv preprint doi: https://doi.org/10.1101/2023.02.24.529908; this version posted February 25, 2023. The copyright holder for this preprint (which was not certified by peer review) is the author/funder, who has granted bioRxiv a license to display the preprint in perpetuity. It is made available under aCC-BY-ND 4.0 International license.

(B) Amplitude and (C) phase responses of the relative displacement, ΔX, between the BM and TM for different amplitudes P_a of the harmonic force $P(t)$. P_a is indicated for each curve. Responses for the condition $K_{\mathrm{tm}} = 0$ are shown only for $P_a = 1$. Vertical black arrows in (C) show changes in the ΔX phase with increasing P_a, i.e. the stimulus level. Numbers in circles in (C) identify presumed frequency positions of the corresponding experimental responses (Figure 2B) relative to ω_{tm} and ω_{bm}. Green horizontal arrows in (C) shows a presumed shift of ω_{tm} and ω_{bm} to lower frequencies due to changes in K_{n}. See inset in (A).

(D) Amplitude and (E) phase angle of BM responses for different amplitudes P_a of the harmonic force $P(t)$. P_a is indicated for each curve. Responses for the condition $K_{\mathrm{tm}} = 0$ are shown only for $P_a = 1$. Vertical black arrows in (E) show changes in the BM phase responses with increasing P_a, i.e. the stimulus level.

Vertical dashed magenta lines indicate ω_{tm} and ω_{bm} as defined by equation (3). A horizontal grey arrow in (B) indicates the frequency range where *in vivo* responses are not recorded because the BM TW does not propagate beyond the ω_{bm} place towards the cochlear apex (Figure 1B).

The following parameters were used to calculate the responses: M_{tm} = 1, M_{bm}= 10, ω_{tm} = 1, ω_{bm} = 1.4, ω_{c} = 5, $\zeta_{\mathrm{tm}}^{+} = \zeta_{\mathrm{bm}}^{+} = 0.15$, $x_1 = 0$, $a_1 = 1$.

Responses of the active model to harmonic excitation $P(t) = P_a \sin(\omega t)$ for different amplitude P_{a} are shown in Figure 4. Only responses below and around ω_{bm} are shown because the BM TW does not propagate beyond the ω_{bm} place towards the cochlear apex (horizontal grey arrow in Figure 4B). Therefore, the second normal mode (see question 2 and an answer to it in the Supplemental Information for detailed derivation), which is shifted to frequencies well above ω_{bm} due to strong elastic coupling K_{c} between M_{tm} and M_{bm}, is not shown in Figure 4 (compare Figure 3B and 4B). An active model, which includes only local BM/TM resonances, provides an impressively good qualitative description of the experimental data for the OHC receptor potentials (Figure 2) despite the absence of global phenomena like the BM TW or elastic/hydromechanical coupling along the cochlea. The RP minimum seen about half an octave below the CF in isolevel RP responses recorded for a stimulus level of 70 dB SPL to ensure the recording of responses over a wide frequency range (Figure 2A) is less sharp than the model minima recorded for smaller P_{a} (Figure 4B). However, the model minimum becomes less sharp for $P_{\mathrm{a}} = 100$ when the nonlinear model amplification becomes saturated (see question 1 and an answer to it in the Supplemental Information for the assessment of the depth of the local minimum at ω_{tm} for varying TM damping).

The active local resonance model provides an explanation of the seemingly complex level-dependent OHC RP amplitude and phase behaviour observed in experiments (Figure 2B, Kössl and Russell, 1992) assuming that ω_{tm} was situated around 13 kHz, i.e. about half an

bioRxiv preprint doi: https://doi.org/10.1101/2023.02.24.529908; this version posted February 25, 2023. The copyright holder for this preprint (which was not certified by peer review) is the author/funder, who has granted bioRxiv a license to display the preprint in perpetuity. It is made available under aCC-BY-ND 4.0 International license.

284 octave below the CF of 18 kHz. Indeed, in this case, the phase angle does not depend on the
285 stimulus level when the stimulus frequency is 8 kHz and well below ω_{tm} (panel 1 in Figure
286 2B and frequency point 1 in Figure 4C). There is a small phase lead with level (leftmost black
287 vertical arrow in Figure 4C) for the stimulus frequency of 11 kHz which is situated closer to
288 but still below ω_{tm} (panel 2 in Figure 2B and frequency point 2 in Figure 4C) but the phase
289 lead is larger (rightmost black vertical arrow in Figure 4C) for the stimulus frequency of 19
290 kHz above the CF/ω_{bm} (panel 6 in Figure 2B and frequency point 6 in Figure 4C). The phase
291 behaviour reverses and the phase lags with level (middle vertical black arrow in Figure 4C)
292 for the stimulus frequency of 15 kHz situated between the ω_{tm} and CF/ω_{bm} (panel 4 in
293 Figure 2B and frequency point 4 in Figure 4C). A reversal of phase behaviour is observed
294 with increasing the stimulus level for 13 kHz (small lead to lag) situated just below assumed
295 ω_{tm}, and 17 kHz (small lag to lead) situated just below the CF/ω_{bm} in panels 3 and 5 in
296 Figure 2B, respectively. At the same time, this reversal of the phase behaviour for both
297 stimulus frequencies are associated with phase transitions which are close to 180°. The near-
298 180° phase transition at 13 kHz is steeper than the transition observed for 17 kHz which is
299 expected because of a steeper phase slope near ω_{tm} (Figure 4C). An amplitude notch in the
300 OHC RP level function is, however, observed only for 13 kHz stimulus (panel 3 in Figure
301 2B) and it is absent at 17 kHz. In terms of the active model (Figure 4A), the observed
302 nonmonotonic amplitude and phase behaviour is explained by presumed shifts of ω_{tm} and
303 ω_{bm} to lower frequencies with increasing the stimulus level (green horizontal arrows in
304 Figure 4C). Indeed, the low-frequency shift of maximum responses near the CF is well-
305 documented (e.g. Robles and Ruggero, 2001) and a low-frequency shift of the TM resonance
306 was suggested from observation of different indices of cochlear responses associated with
307 ω_{tm} (Lukashkin et al., 2007a). Therefore, if 13 kHz (panel 3 in Figure 2B) is situated just
308 below ω_{tm} (frequency point 3 in Figure 4C) for low stimulus levels but it appears above ω_{tm}
309 for high stimulus levels then the ΔX amplitude (i.e. the OHC RP amplitude) would fall into
310 the amplitude minimum at ω_{tm} and eventually recover from it with increasing stimulus level.
311 In this case not only a reversal of the phase behaviour and a steep phase transition but also an
312 amplitude notch in the OHC RP level functions should be observed. The amplitude notch in
313 the OHC RP level functions should not be observed during reversal of the phase behaviour
314 and corresponding phase transition for responses to the 17 kHz stimulus (panel 5 in Figure
315 2B) if this stimulus frequency is situated just below the CF/ω_{bm} (frequency point 5 in Figure
316 4C) at low stimulus levels but appears above CF/ω_{bm} for high stimulus levels due to a low-

bioRxiv preprint doi: https://doi.org/10.1101/2023.02.24.529908; this version posted February 25, 2023. The copyright holder for this preprint (which was not certified by peer review) is the author/funder, who has granted bioRxiv a license to display the preprint in perpetuity. It is made available under aCC-BY-ND 4.0 International license.

frequency shift of ω_{bm} because there is no a local amplitude minimum associated with the ΔX frequency responses near ω_{bm} (Figure 4B).

A local resonance active cochlear model which includes only nonlinear negative damping (Figure 4A) does not reproduce the suggested low-frequency shift of ω_{tm} and ω_{bm} at high stimulus levels (green arrows in Figure 4C). The low-frequency shift of the TM and BM resonances would occur quite naturally if the nonlinear, level-dependent OHC force P_{n} is out of phase with the damping force η_{n} (Figure 4A, insert). In this case nonlinear, level-dependent stiffness K_{n} or inertial M_{n} projections associated with the OHC action that correspond to the imaginary parts of the impedance are observed for mechanical components of the system (e.g. see Kolston et al., 1990). Changes in the projections K_{n} or M_{n} due to changes in the phase angle of P_{n} or variation of its amplitude with increasing stimulus level, would lead to changes in the imaginary part of the components' impedances, thus changing frequencies ω_{tm} and ω_{bm}. Changes in the effective masses or stiffnesses of the system components, and, hence, shifts of ω_{tm} and ω_{bm}, might also be explained by a spread of excitation along the cochlea due to stiffening of the TM or/and entraining larger masses of cochlear fluids with increasing stimulus levels (see Discussion for more details). Also, the shift may be a product of OHC efferent activation (Guinan, 2018) but it should still be associated with changes in the imaginary part of the impedances, i.e. the effective stiffness/mass changes, even in this case.

It is worth noting that the minimal local resonance active cochlear model with negative damping (Figure 4A) also qualitatively reproduces experimental level dependent behaviour of the BM phase. It has been known for a long time that the phase angle of BM responses lags/leads with levels for frequencies below/above the CF/ω_{bm}, respectively (Robles and Ruggero, 2001). Exactly this type of phase behaviour is observed for the local resonance active cochlear model with negative damping (black vertical arrows in Figure 4E).

DISCUSSION

The objective of this study is to find a minimal mechanical system which still can qualitatively explain the behaviour of the OHC RP *in vivo*. It is demonstrated that a local resonance of a strongly coupled TM and BM as suggested by (Allen, 1980; Zwislocki, 1980; Allen and Neely, 1992) and experimentally recorded by (Gummer et al., 1996; Lee et al., 2016) is sufficient to explain the phenomenology of the seemingly complex changes in the OHC RP amplitude and phase recorded close to OHCs *in vivo* for wide range of frequencies

bioRxiv preprint doi: https://doi.org/10.1101/2023.02.24.529908; this version posted February 25, 2023. The copyright holder for this preprint (which was not certified by peer review) is the author/funder, who has granted bioRxiv a license to display the preprint in perpetuity. It is made available under aCC-BY-ND 4.0 International license.

and levels of acoustic stimulation (Kössl and Russell, 1992; Russell and Kössl, 1992; Levic et al., 2022). Moreover, the model reveals that the nonmonotonic amplitude behaviour (i.e. local minima/maxima) of experimentally recorded cochlear responses generated due to radial shear between the TM and OoC at frequencies below the CF, is observed at the TM resonance frequency and the frequency position of these minima/maxima does not depend either on the properties of the pressure driven part of the system (i.e. the BM with the OoC sitting on its top) or the degree of coupling between the TM and OoC. The model confirms that the shear between the TM and OoC is mass dominated in the frequency region associated with nonlinear cochlear amplification and a corresponding phase transition is observed for this frequency region between ω_{tm} and ω_{bm} (Figure 3C, 4C), where the timing of OHC stimulation is optimal for cochlear amplification. An obvious conclusion is that the timing is suboptimal for cochlear amplification and sharpened frequency tuning of mechanical responses of the cochlear partition outside of the range of between ω_{tm} and ω_{bm}, despite the finding that OHCs are stimulated over a wider frequency span than $[\omega_{\mathrm{tm}}, \omega_{\mathrm{bm}}]$ as judged by the reticular lamina active responses (Ren et al., 2016; He et al., 2022).

There is no need for global phenomena, e.g. TW or elastic/hydromechanical coupling along the cochlea, to explain the experimental data on the OHC RP (Figure 2B). In fact, addition of global phenomena to the local resonance model can smear sharp antiresonance/resonance in the system as discussed below. This, however, does not destroy the effect of local resonance. Its signature could still be seen in various types of cochlear responses (Lukashkin et al., 2010). Addition of the TW to the local resonance model, which includes independent TM resonance at frequencies below the BM resonance, provides a good fit to the neural data (Allen, 1980; Allen and Neely, 1992; Allen and Fahey, 1993). A notch of insensitivity seen in the neural data at a frequency about half an octave below the CF (Liberman, 1978; Allen, 1980; Liberman and Dodds, 1984; Taberner and Liberman, 2005; Temchin et al., 2008) resembles a similar notch in the OHC RP (Figure 2A) and in neural suppression tuning curves (Lukashkin et al., 2007a). The notch disappears in mutants with the TM detached from the spiral limbus (Lukashkin et al., 2012), confirming its origin (compare with the red curve for $K_{\mathrm{tm}} = 0$ in Figure 3B). It was also suggested that the amplitude and phase dependence of the distortion product otoacoustic emission (DPOAE) on the ratio of the two primary stimulus tones (f1 and f2, f2 > f1) used to evoke the DPOAEs, reflected band-pass filtering of the DPOAEs by the mechanical filter associated with the local TM resonance. Amplitude maxima for DPOAEs of different order (i.e. 2f1-f2, 3f1-2f2, 4f1-3f2) are observed at the

bioRxiv preprint doi: https://doi.org/10.1101/2023.02.24.529908; this version posted February 25, 2023. The copyright holder for this preprint (which was not certified by peer review) is the author/funder, who has granted bioRxiv a license to display the preprint in perpetuity. It is made available under aCC-BY-ND 4.0 International license.

same frequency which is independent of the f2/f1 ratio (Brown et al., 1992; Allen and Fahey, 1993) and the phase of DPOAE of different order changes from lag to lead at the same frequency when the levels of primaries are increased (Lukashkin and Russell, 2003; Lukashkin et al., 2007a).

The local minimum in sensitivity of the OHC RP at frequencies about half an octave below the CF (Figure 2A) and corresponding amplitude notches associated with steep phase transitions (panel 3 in Figure 2B) are more sharply tuned in intracellular OHC RP recordings or extracellular recordings in the closest vicinity of OHCs (Kössl and Russell, 1992; Russell and Kössl, 1992; Levic et al., 2022) than when measured from the OoC fluid space (Fridberger et al., 2004) and close to the BM as a cochlear microphonic (Dong and Olson, 2013), when it becomes increasingly broader and less distinct with increasing stimulation levels. We attribute this difference to two effects, namely, to the level-dependent increase in the damping as illustrated in Figure 4B and to the level-dependent increase in the numbers of generators (OHCs) contributing to the extracellular signal (Patuzzi et al., 1989) that smears the phase data, rather than to the single effect of fluid damping, as has been recently suggested and modelled based on cochlear microphonic measurements (Nankali et al., 2020). The same level-dependent summation of electrical signals from a gradually increasing number of generators leading to a partial phase cancellation might explain lack of an obvious low-frequency shift of the minimum in the gross OHC electrical responses (Fridberger et al., 2004; Dong and Olson, 2013), the shift was suggested to explain the level dependent behaviour of different indices of cochlear responses associated with the TM resonance (Lukashkin et al., 2007a) and the OHC RP data (green arrows in Figure 4C).

It was suggested that a low-frequency shift of ω_{tm} and ω_{bm} (green arrows in Figure 4C), and corresponding shift of the low-frequency minimum of OHC RP and its local maximum near the CF with increasing the sound intensity might occur due to the desynchronization of the nonlinear, level-dependent OHC force P_{n} contributing to the imaginary parts of the mechanical impedances of the components (insert in Figure 4A). There are two additional mechanisms which might contribute to the low-frequency shift. Vibration of an individual element within the cochlea generates a near field pressure, which increases the element's effective mass (Ni and Elliott, 2015). Increase in the TW wavelength with sound intensity might increase the fluid-loaded mass on the individual elements (Steele and Taber, 1979; Elliott et al., 2022; Nankali et al., 2022), thus, lowering their resonance frequencies (Equation 3). Also, the TM material properties are frequency and, thus, velocity dependent and the TM

bioRxiv preprint doi: https://doi.org/10.1101/2023.02.24.529908; this version posted February 25, 2023. The copyright holder for this preprint (which was not certified by peer review) is the author/funder, who has granted bioRxiv a license to display the preprint in perpetuity. It is made available under aCC-BY-ND 4.0 International license.

shear storage modulus increases with stimulation frequency/velocity, especially at the cochlear base (Jones et al., 2013). Increase in the TM velocity response with stimulus level and resultant TM stiffening might lead to larger regions of the TM and OoC being involved in local OHC excitation due to increased elastic coupling along the TM (Dewey et al., 2018). This would manifest in larger M_{tm} and M_{bm}, and corresponding decrease in ω_{tm} and ω_{bm}.

It should be noted that the OHC RP data which are analysed in this study were obtained from the high-frequency cochlear base. Both the mechanical (Recio-Spinoso and Oghalai, 2017; Burwood et al., 2022) and neural (Liberman, 1978; Allen, 1980; Liberman and Dodds, 1984; Taberner and Liberman, 2005; Temchin et al., 2008) responses at the extreme low-frequency cochlear apex have much broader tuning and lack a low-frequency shoulder, and neural responses have no local sensitivity minimum below the CF. In fact, a large stretch of the cochlear partition at the extreme apex moves in phase, making phase-locking of neural responses (Rose et al., 1967; Kim and Molnar, 1979; Johnson, 1980; Palmer and Russell, 1986) a preferable mechanism of frequency coding in this cochlear region. The difference in responses between the base and apex possibly reflects the relative difference in mechanical properties of cochlear structures. The dimensions of the TM vary along the length of the cochlea; its radial width and cross-sectional area and, hence, linear mass density increase from the basal to the apical end of the cochlea (Richardson et al., 2008). The lengths of the OHC hair bundles increase from the cochlear base to apex (Wright, 1984; Yarin et al., 2014), which results in a decrease of their rotational stiffness (Tobin et al., 2019; Miller et al., 2021) and, thus, reduction in elastic coupling between the TM and OoC.

Limitations of the study

The objective of this work is to find a minimal model which still can qualitatively explain the complex behaviour of the OHC RP for different levels and frequencies of stimulation below and around the CF at the high frequency cochlear base. For this purpose, the model does not include global phenomena, e.g. TW along the BM and elastic coupling along the cochlear partition, and it cannot be used to fit experimental data. Only the qualitative behaviour of the OHC RP amplitude and phase responses is considered. The model assumes uniform negative damping/cochlear amplification over the entire frequency range, which, however, does not affect the conclusions because the conclusions are based on the OHC RP behaviour around the frequency range of $[\omega_{\mathrm{tm}}, \omega_{\mathrm{bm}}]$ where nonlinear cochlear amplification is observed. Also,

bioRxiv preprint doi: https://doi.org/10.1101/2023.02.24.529908; this version posted February 25, 2023. The copyright holder for this preprint (which was not certified by peer review) is the author/funder, who has granted bioRxiv a license to display the preprint in perpetuity. It is made available under aCC-BY-ND 4.0 International license.

446 the model explains OHC RPs recorded at the high-frequency cochlear region and responses at
447 the extreme low-frequency cochlear apex might not be well explained.

448 **METHODS**

449 MATLAB (The MathWorks. Inc. 2022a) was used to find solutions for the linear (Figure 3)
450 and nonlinear (Figure 4) models in the time domain for a harmonic stimulation $P(t) =$
451 $P_{\mathrm{a}}\sin(\omega t)$ and the fast Fourier transform was applied to the solutions to extract the
452 component at frequency ω.

453 **ACKNOWLEDGMENTS**

454 This work was funded by United Kingdom Medical Research Council Grant MR/W028956/1.
455 OR is supported by the UKRI Future Leaders Fellowship (Grant MR/T043326/1).

456 **AUTHOR CONTRIBUTIONS**

457 IR and ANL conceived and designed the study. OR completed the analytical analysis of the
458 mechanical systems. ANL performed computational simulations. All authors wrote the
459 manuscript.

460 **DECLARATION OF INTERESTS**

461 The authors declare that they have no known competing financial interests or personal
462 relationships that could have appeared to influence the work reported in this paper.

463 **REFERENCES**

464 Allen, J.B. (1980). Cochlear micromechanics – A physical model of transduction. J. Acoust.
465 Soc. Am. *68*, 1660–1670.

466 Allen, J.B., and Fahey, P.F. (1993). A second cochlear frequency map that correlates
467 distortion product and neural tuning measurement. J. Acoust. Soc. Am. *94*, 809–817.

468 Ashmore, J.F. (1987). A fast motile response in guinea-pig outer hair cells: the cellular basis
469 of the cochlear amplifier. J. Physiol. (Lond.) *388*, 323-347.

470 Ashmore, J.F. (2008). Cochlear outer hair cell motility. Physiol. Rev. *88*, 173–210.

471 von Békésy, G. (1960). Experiments in hearing. (McGraw–Hill).

472 Brownell, W.E., Bader, C.R., Bertrand, D., and de Ribaupierre, Y. (1985). Evoked
473 mechanical responses of isolated cochlear outer hair cells. Science *227*, 194–196.

474 Burwood, G., Hakizimana, P., Nuttall, A. L., and Fridberger, A. (2022). Best frequencies and
475 temporal delays are similar across the low-frequency regions of the guinea pig cochlea. Sci.
476 Adv. *8*, eabq2773.

bioRxiv preprint doi: https://doi.org/10.1101/2023.02.24.529908; this version posted February 25, 2023. The copyright holder for this preprint (which was not certified by peer review) is the author/funder, who has granted bioRxiv a license to display the preprint in perpetuity. It is made available under aCC-BY-ND 4.0 International license.

Burwood, G., He, W.X., Fridberger, A., Ren, T.Y., and Nuttall, A.L. (2021). Outer hair cell driven reticular lamina mechanical distortion in living cochleae. Hear. Res. *423*, 108405.

Dallos, P. (2008). Cochlear amplification, outer hair cells and prestin. Curr. Opin. Neurobiol. *18*, 370–376.

Davis H. (1983). An active process in cochlear mechanics. Hear. Res. *9*, 79–90.

Dewey, J.B., Xia, A., Müller, U., Belyantseva, I.A., Applegate, B.E., and Oghalai, J.S. (2018). Mammalian auditory hair cell bundle stiffness affects frequency tuning by increasing coupling along the length of the cochlea. Cell Rep. *23*, 2915– 2927.

Dewey, J.B., Altoè, A., Shera, C.A., Applegate, B.E., and Oghalai, J.S. (2021). Cochlear outer hair cell electromotility enhances organ of Corti motion on a cycle-by-cycle basis at high frequencies *in vivo*. Proc. Natl. Acad. Sci. USA *118*, e2025206118.

Dong, W., and Olson, E.S. (2013). Detection of cochlear amplification and its activation. Biophys. J. *105*, 1067–1078.

Elliott, S.J., Tehrani, M.G., and Langley, R.S. (2015). Nonlinear damping and quasi-linear modelling. Phil. Trans. R. Soc. A *373*, 20140402.

Elliott, S.J., Marrocchio, R., and Grosh, K. (2022). Forms of longitudinal coupling in the organ of Corti. Mechanics of Hearing Workshop, 24-29 July, Denmark.

Fridberger, A., de Monvel, J.B., Zheng, J., Hu, N., Zou, Y., Ren, T., and Nuttall, A.L. (2004). Organ of Corti potentials and the motion of the basilar membrane. J. Neurosci. *24*, 10057–10063.

Gold, T. (1948). Hearing. II. The physical basis of the action of the cochlea. Proc. R. Soc. Lond. B. Biol. Sci. *135*, 492–498.

Guinan Jr, J.J. (2018). Olivocochlear efferents: Their action, effects, measurement and uses, and the impact of the new conception of cochlear mechanical responses. Hear. Res. *362*, 38-47.

Gummer, A.W., Hemmert, W., and Zenner, H.P. (1996). Resonant tectorial membrane motion in the inner ear: its crucial role in frequency tuning. Proc. Natl. Acad. Sci. USA 93, 8727–8732.

He, W., Burwood, G., Fridberger, A., Nuttall, A. L., and Ren, T. (2022). An outer hair cell-powered global hydromechanical mechanism for cochlear amplification. Hear. Res. *423*, 108407.

He, W., Burwood, G., Porsov, E.V., Fridberger, A., Nuttall, A.L., and Ren, T. (2022). The reticular lamina and basilar membrane vibrations in the transverse direction in the basal turn of the living gerbil cochlea. Sci. Rep. *12*, 19810.

Johnson, D.H. (1980). The relationship between spike rate and synchrony in responses of auditory-nerve fibers to single tones. J. Acoust. Soc. Am. *68*, 1115-1122.

Jones GP, Lukashkina VA, Russell IJ, Elliott SJ, and Lukashkin AN (2013). Frequency-dependent properties of the tectorial membrane facilitate energy transmission and amplification in the cochlea. Biophys. J. *104*, 1357–1366.

bioRxiv preprint doi: https://doi.org/10.1101/2023.02.24.529908; this version posted February 25, 2023. The copyright holder for this preprint (which was not certified by peer review) is the author/funder, who has granted bioRxiv a license to display the preprint in perpetuity. It is made available under aCC-BY-ND 4.0 International license.

Kim, D.O., and Molnar, C.E. (1979). A population study of cochlear nerve fibers: comparison of spatial distributions of average-rate and phase-locking measures of responses to single tones. J. Neurophysiol. *42*, 16-30.

Kolston, P.J., de Boer, E., Viergever, M.A., and Smoorenburg, G.F. (1990). What type of force does the cochlear amplifier produce? J. Acoust. Soc. Am. *88*, 1794-1801.

Kössl M, Russell IJ (1992). The phase and magnitude of hair cell receptor potentials and frequency tuning in the guinea pig cochlea. J. Neurosci. *12*, 1575-1586.

Lee, H.Y., Raphael, P.D., Xia, A., Kim, J., Grillet, N., Applegate, B.E., Bowden, A.K.E., and Oghalai, J.S. (2016). Two-dimensional cochlear micromechanics measured in vivo demonstrate radial tuning within the mouse organ of Corti. J. Neurosci. *36*, 8160–8173.

Levic S, Lukashkina VA, Simões P, Lukashkin AN, Russell IJ (2022). A gap-junction mutation reveals that outer hair cell extracellular receptor potentials drive high-frequency cochlear amplification. J. Neurosci. *42*, 7875-7884.

Liberman, M.C. (1978). Auditory-nerve response from cats raised in a low-noise chamber. J. Acoust. Soc. Am. *63*, 442–455.

Liberman, M.C., and Dodds, L.W. (1984). Single-neuron labeling and chronic cochlear pathology. III. Stereocilia damage and alterations of threshold tuning curves. Hear. Res. *16*, 55–74.

Liberman, M.C., Gao, J., He, D.Z.Z., Wu, X., Jia, S., and Zuo, J. (2002). Prestin is required for electromotility of the outer hair cell and for the cochlear amplifier. Nature *419*, 300–304.

Lukashkin, A.N., Lukashkina, V.A., Legan, K.P., Richardson, G.P., and Russel, I.J. (2004). Role of the tectorial membrane revealed by otoacoustic emissions recorded from wild-type and transgenic *Tecta*$^{ENT/ENT}$ mice. J. Neurophysiol. *91*, 163–171.

Lukashkin, A.N., Richardson, G.P., and Russell, I.J. (2010). Multiple roles for the tectorial membrane in the active cochlea. Hear. Res. *266*, 26-35.

Lukashkin, A.N., and Russell, I.J. (1999). Analysis of the f2–f1 and 2f1–f2 distortion components generated by the hair cell mechano-electrical transducer: dependence on the amplitudes of the primaries and feedback gain. J. Acoust. Soc. Am. *106*, 2661–2668.

Lukashkin, A.N., and Russell, I.J. (2003). A second, low frequency mode of vibration in the intact mammalian cochlea. J. Acoust. Soc. Am. *113*, 1544–1550.

Lukashkin, A.N., Smith, J.K., and Russell, I.J. (2007a). Properties of distortion product otoacoustic emissions and neural suppression tuning curves attributable to the tectorial membrane resonance. J. Acoust. Soc. Am. *121*, 337-343.

Lukashkin, A.N., Walling, M.N., and Russell, I.J. (2007b). Power amplification in the mammalian cochlea. Curr. Biol. *17*, 1340-1344.

Meaud, J., and Grosh, K. (2010). The effect of tectorial membrane and basilar membrane longitudinal coupling in cochlear mechanics. J. Acoust. Soc. Am. *127*, 1411–1421.

Meaud, J., and Grosh, K. (2014). Effect of the attachment of the tectorial membrane on cochlear micromechanics and two-tone suppression. Biophys. J. *106*, 1398–1405.

bioRxiv preprint doi: https://doi.org/10.1101/2023.02.24.529908; this version posted February 25, 2023. The copyright holder for this preprint (which was not certified by peer review) is the author/funder, who has granted bioRxiv a license to display the preprint in perpetuity. It is made available under aCC-BY-ND 4.0 International license.

Mellado Lagarde, M.M., Drexl, M., Lukashkina, V.A., Lukashkin, A.N., and Russell. I.J. (2008). Outer hair cell somatic, not hair bundle, motility is the basis of the cochlear amplifier. Nat. Neurosci. *11*, 746–748.

Miller, K. K., Atkinson, P., Mendoza, K. R., Ó Maoiléidigh, D., and Grillet, N. (2021). Dimensions of a living cochlear hair bundle. Front. Cell Dev. Biol. *9*, 742529.

Nankali, A., Wang, Y., Strimbu, C.E., Olson, E.S., and Grosh, K. (2020). A role for tectorial membrane mechanics in activating the cochlear amplifier. Sci. Rep. *10*, 17620.

Nankali, A., Shera, C.A., Applegate, B.E., and Oghalai, J.S. (2022). Interplay between traveling wave propagation and amplification at the apex of the mouse cochlea. Biophys. J. *121*, 2940-2951.

Ni, G., and Elliott, S.J. (2015). Comparing methods of modeling near field fluid coupling in the cochlea. J. Acoust. Soc. Am. *137*, 1309-1317.

Nilsen, K.E., and Russell, I.J. (1999). Timing of cochlear feedback: spatial and temporal representation of a tone across the basilar membrane. Nat. Neurosci. *2*, 642–648.

Nowotny, M., and Gummer, A.W. (2006). Nanomechanics of the subtectorial space caused by electromechanics of cochlear outer hair cells. Proc. Natl. Acad. Sci. USA *103*, 2120–2125.

Palmer, A.R., and Russell, I.J. (1986). Phase-locking in the cochlear nerve of the guinea-pig and its relation to the receptor potential of inner hair-cells. Hear. Res. *24*, 1-15.

Patuzzi, R.B., and Yates, G.K. (1987). The low-frequency response of inner hair cells in the guinea pig cochlea: implications for fluid coupling and resonance of the stereocilia. Hear. Res. *30*, 83-98.

Patuzzi, R.B., Yates, G.K., and Johnstone, B.M. (1989). The origin of the low-frequency microphonic in the first cochlear turn of guinea-pig. Hear. Res. *39*, 177– 188.

Recio-Spinoso, A., and Oghalai, J.S. (2017). Mechanical tuning and amplification within the apex of the guinea pig cochlea. J. Physiol. (Lond.) *595*, 4549-4561.

Ren, T., He, W., and Kemp, D. (2016). Reticular lamina and basilar membrane vibrations in living mouse cochleae. Proc. Natl. Acad. Sci. USA *113*, 9910–9915.

Richardson, G.P., Lukashkin, A.N., and Russell, I. J. (2008). The tectorial membrane: one slice of a complex cochlear sandwich. Curr. Opin. Otolaryngol. Head Neck Surg. *16*, 458–464.

Robles, L., and Ruggero, M.A. (2001). Mechanics of the mammalian cochlea. Physiol. Rev. *81*, 1305–1352.

Rose, J.E., Brugge, J.F., Anderson, D.J., and Hind, J.E. (1967). Phase-locked response to low-frequency tones in single auditory nerve fibers of the squirrel monkey. J. Neurophysiol. *30*, 769-793.

Russell, I.J. (2008). Cochlear receptor potentials. In: The Senses: A Comprehensive Reference, edited by A. I. Basbaum, A. Kaneko, G. M. Shepherd, G. Westheimer, T. D. Albright, R. H. Masland, et al. Academic Press 2008 Vol. 3, p. 3019-358.

Russell, I.J., and Kössl, M. (1992). Modulation of hair cell voltage responses to tones by low-frequency biasing of the basilar membrane in the guinea pig cochlea. J. Neurosci. *12*,1587–1601.

bioRxiv preprint doi: https://doi.org/10.1101/2023.02.24.529908; this version posted February 25, 2023. The copyright holder for this preprint (which was not certified by peer review) is the author/funder, who has granted bioRxiv a license to display the preprint in perpetuity. It is made available under aCC-BY-ND 4.0 International license.

Santos-Sacchi, J., and Dilger, J.P. (1988). Whole cell currents and mechanical responses of isolated outer hair cells. Hear. Res. *35*, 143–150.

Sellick, P.M., and Russell, I.J. (1980). The responses of inner hair cells to basilar membrane velocity during low frequency auditory stimulation in the guinea pig cochlea. Hear. Res. *2*, 439-445.

Steele, C.R., and Taber, L.A. (1979). Comparison of WKB calculations and experimental results for three-dimensional cochlear models. J. Acoust. Soc. Am. *65*, 1007–1018.

Taberner, A.M., and Liberman, M.C. (2005). Response properties of single auditory nerve fibers in the mouse. J. Neurophysiol. *93*, 557-569.

Temchin, A.N., Rich, N.C., and Ruggero, M.A. (2008). Threshold tuning curves of chinchilla auditory-nerve fibers I dependence on characteristic frequency and relation to the magnitudes of cochlear vibrations. J. Neurophysiol. *100*, 2889–2898.

Tobin, M., Chaiyasitdhi, A., Michel, V., Michalski, N., and Martin, P. (2019). Stiffness and tension gradients of the hair cell's tip-link complex in the mammalian cochlea. eLife, *8*, e43473.

Wright, A. (1984). Dimensions of the cochlear stereocilia in man and the guinea pig. Hear. Res. *13*, 89–98

Yarin, Y.M., Lukashkin, A.N., Poznyakovskiy, A.A., Meißner, H., Fleischer, M., Baumgart, J., ... and Zahnert, T. (2014). Tonotopic morphometry of the lamina reticularis of the guinea pig cochlea with associated microstructures and related mechanical implications. JARO, *15*, 1-11.

Zheng, J., Deo, N., Zou, Y., Grosh, K., and Nuttall, A.L. (2007). Chlorpromazine alters cochlear mechanics and amplification: In vivo evidence for a role of stiffness modulation in the organ of Corti. J. Neurophysiol. *97*, 994–1004.

Zwislocki, J.J. (1980). Theory of cochlear mechanics. Hear. Res. *2*, 171–182.

Supplemental information

We would like to analyse the system of equations (4, 5) to answer the following questions:

1. What is the condition for a minimum of ΔX at ω_{tm} to occur?
2. What is contribution of the normal modes into the response?
3. Does the ΔX minimum occur when K_{tm} is absent, i.e. when there is no limbal attachment of the TM to the spiral limbus?

To answer the question 1, and using the complex-exponential method, the equations (4, 5) can be rewritten

$$\frac{d^2 Z_{\mathrm{bm}}}{dt^2} + \zeta_{\mathrm{bm}} \frac{dZ_{\mathrm{bm}}}{dt} + \omega_{\mathrm{bm}}^2 Z_{\mathrm{bm}} - \omega_{\mathrm{c}}^2 (Z_{\mathrm{tm}} - Z_{\mathrm{bm}}) \left(\frac{M_{\mathrm{tm}}}{M_{\mathrm{bm}}}\right) = -i \frac{P_{\mathrm{a}}}{M_{\mathrm{bm}}} e^{i\omega t}, \qquad \text{(S1)}$$

and

bioRxiv preprint doi: https://doi.org/10.1101/2023.02.24.529908; this version posted February 25, 2023. The copyright holder for this preprint (which was not certified by peer review) is the author/funder, who has granted bioRxiv a license to display the preprint in perpetuity. It is made available under aCC-BY-ND 4.0 International license.

$$\frac{d^2Z_{\mathrm{tm}}}{dt^2} + \zeta_{\mathrm{tm}}\frac{dZ_{\mathrm{tm}}}{dt} + \omega_{\mathrm{tm}}^2 Z_{\mathrm{tm}} + \omega_{\mathrm{c}}^2(Z_{\mathrm{tm}} - Z_{\mathrm{bm}}) = 0. \quad \text{(S2)}$$

Let us assume the steady state solution in the following form:

$$Z_{\mathrm{bm}} = A_{\mathrm{bm}}e^{i(\omega t - \delta_{\mathrm{bm}})},$$
$$Z_{\mathrm{tm}} = A_{\mathrm{tm}}e^{i(\omega t - \delta_{\mathrm{tm}})}, \quad \text{(S3)}$$

with $X_{\mathrm{bm}} = Re(Z_{\mathrm{bm}})$ and $X_{\mathrm{tm}} = Re(Z_{\mathrm{tm}})$.

Substituting expressions (S3) for Z_{bm} and Z_{tm} into equations (S1, S2) yields

$$A_{\mathrm{bm}}e^{i(\omega t - \delta_{\mathrm{bm}})}\left(-\omega^2 + i\zeta_{\mathrm{bm}}\omega + \left(\omega_{\mathrm{bm}}^2 + \omega_{\mathrm{c}}^2\frac{M_{\mathrm{tm}}}{M_{\mathrm{bm}}}\right)\right) - \omega_{\mathrm{c}}^2\frac{M_{\mathrm{tm}}}{M_{\mathrm{bm}}}A_{\mathrm{tm}}e^{i(\omega t - \delta_{\mathrm{tm}})} = -i\frac{P_{\mathrm{a}}}{M_{\mathrm{bm}}}e^{i\omega t} \quad \text{(S4)}$$

$$A_{\mathrm{tm}}e^{i(\omega t - \delta_{\mathrm{tm}})}\left(-\omega^2 + i\zeta_{\mathrm{tm}}\omega + (\omega_{\mathrm{tm}}^2 + \omega_{\mathrm{c}}^2)\right) - \omega_{\mathrm{c}}^2 A_{\mathrm{bm}}e^{i(\omega t - \delta_{\mathrm{bm}})} = 0, \quad \text{(S5)}$$

and after re-arranging

$$A_{\mathrm{bm}}e^{-i\delta_{\mathrm{bm}}}\left(-\omega^2 + i\zeta_{\mathrm{bm}}\omega + \left(\omega_{\mathrm{bm}}^2 + \omega_{\mathrm{c}}^2\frac{M_{\mathrm{tm}}}{M_{\mathrm{bm}}}\right)\right) - \omega_{\mathrm{c}}^2\frac{M_{\mathrm{tm}}}{M_{\mathrm{bm}}}A_{\mathrm{tm}}e^{-i\delta_{\mathrm{tm}}} = -i\frac{P_{\mathrm{a}}}{M_{\mathrm{bm}}}, \quad \text{(S6)}$$

$$A_{\mathrm{tm}}e^{-i\delta_{\mathrm{tm}}}\left(-\omega^2 + i\zeta_{\mathrm{tm}}\omega + (\omega_{\mathrm{tm}}^2 + \omega_{\mathrm{c}}^2)\right) - \omega_{\mathrm{c}}^2 A_{\mathrm{bm}}e^{-i\delta_{\mathrm{bm}}} = 0. \quad \text{(S7)}$$

From equation (S7), we have

$$A_{\mathrm{tm}}e^{-i\delta_{\mathrm{tm}}}\left(-\omega^2 + i\zeta_{\mathrm{tm}}\omega + (\omega_{\mathrm{tm}}^2 + \omega_{\mathrm{c}}^2)\right) = \omega_{\mathrm{c}}^2 A_{\mathrm{bm}}e^{-i\delta_{\mathrm{bm}}} \quad \text{(S8)}$$

or

$$A_{\mathrm{tm}}e^{-i\delta_{\mathrm{tm}}}\left(-\omega^2 + i\zeta_{\mathrm{tm}}\omega + (\omega_{\mathrm{tm}}^2 + \omega_{\mathrm{c}}^2)\right) = \omega_{\mathrm{c}}^2 A_{\mathrm{bm}}e^{-i\delta_{\mathrm{bm}}}. \quad \text{(S9)}$$

Denote $re^{-i\theta} = -\omega^2 + i\zeta_{\mathrm{tm}}\omega + (\omega_{\mathrm{tm}}^2 + \omega_{\mathrm{c}}^2)$, where $r^2 = (-\omega^2 + \omega_{\mathrm{tm}}^2 + \omega_{\mathrm{c}}^2)^2 + \zeta_{\mathrm{tm}}^2\omega^2$ and

$$-\theta = \mathrm{atan2}(\zeta_{\mathrm{tm}}\omega, -\omega^2 + \omega_{\mathrm{tm}}^2 + \omega_{\mathrm{c}}^2), \quad \text{(S10)}$$

where atan2 is a four-quadrant inverse tangent, then

$$A_{\mathrm{tm}}e^{-i\delta_{\mathrm{tm}}}re^{-i\theta} = \omega_{\mathrm{c}}^2 A_{\mathrm{bm}}e^{-i\delta_{\mathrm{bm}}}, \text{or} \quad \text{(S11)}$$

$$A_{\mathrm{tm}}re^{-i(\delta_{\mathrm{tm}}+\theta)} = \omega_{\mathrm{c}}^2 A_{\mathrm{bm}}e^{-i\delta_{\mathrm{bm}}}, \text{or} \quad \text{(S12)}$$

$$A_{\mathrm{tm}} = \omega_{\mathrm{c}}^2\frac{A_{\mathrm{bm}}}{r}, \text{and} \quad \text{(S13)}$$

bioRxiv preprint doi: https://doi.org/10.1101/2023.02.24.529908; this version posted February 25, 2023. The copyright holder for this preprint (which was not certified by peer review) is the author/funder, who has granted bioRxiv a license to display the preprint in perpetuity. It is made available under aCC-BY-ND 4.0 International license.

$$\delta_{\mathrm{tm}} = \delta_{\mathrm{bm}} - \theta. \tag{S14}$$

Local minimum of ΔX is observed when the amplitudes and phases of Z_{bm} and Z_{tm} are close. Let us compare pairs A_{tm} and A_{bm}, δ_{tm} and δ_{bm} in (S13, S14). In case of light damping, $\zeta_{\mathrm{bm}}, \zeta_{\mathrm{tm}} \ll \omega_{\mathrm{bm}}, \omega_{\mathrm{tm}}, \omega_{\mathrm{c}}$. Therefore, from the definitions (S10) of r, when $\omega = \omega_{\mathrm{tm}}$, r is close to ω_{c}^2 (the difference $r - \omega_{\mathrm{c}}^2$ is proportional to $\zeta_{\mathrm{tm}} \ll 1$) and from (S13) $A_{\mathrm{tm}} \cong A_{\mathrm{bm}}$. Also, since $\zeta_{\mathrm{tm}} \ll 1$, from the definition (S10) of θ, when $\omega = \omega_{\mathrm{tm}}$, $-\theta$ is proportional to $\zeta_{\mathrm{tm}}\omega_{\mathrm{tm}}/\omega_{\mathrm{c}}^2$, which is a small value as well, and $\delta_{\mathrm{tm}} \cong \delta_{\mathrm{bm}}$. To summarise, when $\omega = \omega_{\mathrm{tm}}$, amplitudes A_{tm} and A_{bm}, and phases δ_{tm} and δ_{bm} of X_{tm} and X_{bm} are close, and their difference $\Delta X \to 0$ when $\zeta_{\mathrm{tm}} \to 0$.

Note that from the definition of θ (S10), it follows that at $\omega = \sqrt{\omega_{\mathrm{tm}}^2 + \omega_{\mathrm{c}}^2}$, θ changes its value from 0 to $-\pi$. In other words, and if neglecting small terms, this can be rewritten as

$$\delta_{\mathrm{tm}} = \delta_{\mathrm{bm}}, \text{when } \omega^2 < \omega_{\mathrm{tm}}^2 + \omega_{\mathrm{c}}^2; \text{ and } \delta_{\mathrm{tm}} = \delta_{\mathrm{bm}} + \pi, \text{when } \omega^2 > \omega_{\mathrm{tm}}^2 + \omega_{\mathrm{c}}^2.$$

The modelling results support this outcome, see Figure 3E, where the phases of TM and BM responses coincide until $\omega = \sqrt{\omega_{\mathrm{tm}}^2 + \omega_{\mathrm{c}}^2}$, after which there is a jump in the value between the phases by π.

After substituting notations introduced in (S13) and (S14), to (S6), we have

$$A_{\mathrm{bm}} e^{-i\delta_{\mathrm{bm}}} \left(-\omega^2 + i\zeta_{\mathrm{bm}}\omega + \left(\omega_{\mathrm{bm}}^2 + \omega_{\mathrm{c}}^2 \frac{M_{\mathrm{tm}}}{M_{\mathrm{bm}}} \right) \right) - \omega_{\mathrm{c}}^4 \frac{M_{\mathrm{tm}}}{M_{\mathrm{bm}}} \frac{A_{\mathrm{bm}}}{r} e^{-i(\delta_{\mathrm{bm}} - \theta)} = -i \frac{P_{\mathrm{a}}}{M_{\mathrm{bm}}}, \tag{S15}$$

As in the analysis above, let us introduce new variables as follows

$$r_1 e^{-i\theta_1} = -\omega^2 + i\zeta_{\mathrm{bm}}\omega + \left(\omega_{\mathrm{bm}}^2 + \omega_{\mathrm{c}}^2 \frac{M_{\mathrm{tm}}}{M_{\mathrm{bm}}} \right). \tag{S16}$$

Then (S15) takes form

$$A_{\mathrm{bm}} e^{-i\delta_{\mathrm{bm}}} r_1 e^{-i\theta_1} - \omega_{\mathrm{c}}^4 \frac{M_{\mathrm{tm}}}{M_{\mathrm{bm}}} \frac{A_{\mathrm{bm}}}{r} e^{-i(\delta_{\mathrm{bm}} - \theta)} = -i \frac{P_{\mathrm{a}}}{M_{\mathrm{bm}}}, \text{or} \tag{S17}$$

$$A_{\mathrm{bm}} e^{-i\delta_{\mathrm{bm}}} \left(r_1 e^{-i\theta_1} - \frac{\omega_{\mathrm{c}}^4}{r} \frac{M_{\mathrm{tm}}}{M_{\mathrm{bm}}} e^{i\theta} \right) = \frac{P_{\mathrm{a}}}{M_{\mathrm{bm}}} e^{-i\pi/2}. \tag{S18}$$

Denote

$$r_2 e^{i\theta_2} = r_1 e^{-i\theta_1} - \frac{\omega_{\mathrm{c}}^4}{r} \frac{M_{\mathrm{tm}}}{M_{\mathrm{bm}}} e^{i\theta}. \tag{S19}$$

bioRxiv preprint doi: https://doi.org/10.1101/2023.02.24.529908; this version posted February 25, 2023. The copyright holder for this preprint (which was not certified by peer review) is the author/funder, who has granted bioRxiv a license to display the preprint in perpetuity. It is made available under aCC-BY-ND 4.0 International license.

Then (S18) takes form

$$A_{\mathrm{bm}} r_2 e^{-i(\delta_{\mathrm{bm}}-\theta_2)} = \frac{P_{\mathrm{a}}}{M_{\mathrm{bm}}} e^{-i\pi/2}, \tag{S20}$$

from which it follows that

$$A_{\mathrm{bm}} r_2 = \frac{P_{\mathrm{a}}}{M_{\mathrm{bm}}}, \text{and } \delta_{\mathrm{bm}} = \theta_2 + \frac{\pi}{2}. \tag{S21}$$

Recall from (S19),

$$\theta_2 = \mathrm{atan2}\left(-r_1 \sin\theta_1 - \frac{\omega_{\mathrm{c}}^4}{r}\frac{M_{\mathrm{tm}}}{M_{\mathrm{bm}}}\sin\theta, r_1\cos\theta_1 - \frac{\omega_{\mathrm{c}}^4}{r}\frac{M_{\mathrm{tm}}}{M_{\mathrm{bm}}}\cos\theta\right).$$

In order to understand behaviour of the phase θ_2, let's consider the arguments of the atan2 function. After substituting all the notations used in the derivation, we have

$$\begin{aligned}
&-r_1\sin\theta_1 - \frac{\omega_{\mathrm{c}}^4}{r}\frac{M_{\mathrm{tm}}}{M_{\mathrm{bm}}}\sin\theta \\
&= -r_1 \sin\left(-\mathrm{atan2}\left(\zeta_{\mathrm{bm}}\omega, -\omega^2 + \omega_{\mathrm{bm}}^2 + \omega_{\mathrm{c}}^2\frac{M_{\mathrm{tm}}}{M_{\mathrm{bm}}}\right)\right) \\
&- \frac{\omega_{\mathrm{c}}^4}{r}\frac{M_{\mathrm{tm}}}{M_{\mathrm{bm}}}\sin\left(-\mathrm{atan2}(\zeta_{\mathrm{tm}}\omega, -\omega^2 + \omega_{\mathrm{tm}}^2 + \omega_{\mathrm{c}}^2)\right) \\
&= r_1 \sin\left(\mathrm{atan2}\left(\zeta_{\mathrm{bm}}\omega, -\omega^2 + \omega_{\mathrm{bm}}^2 + \omega_{\mathrm{c}}^2\frac{M_{\mathrm{tm}}}{M_{\mathrm{bm}}}\right)\right) \\
&+ \frac{\omega_{\mathrm{c}}^4}{r}\frac{M_{\mathrm{tm}}}{M_{\mathrm{bm}}}\sin\left(\mathrm{atan2}(\zeta_{\mathrm{tm}}\omega, -\omega^2 + \omega_{\mathrm{tm}}^2 + \omega_{\mathrm{c}}^2)\right) = r_1\frac{\zeta_{\mathrm{bm}}\omega}{r_1} + \frac{\omega_{\mathrm{c}}^4}{r}\frac{M_{\mathrm{tm}}}{M_{\mathrm{bm}}}\frac{\zeta_{\mathrm{tm}}\omega}{r} \\
&= \zeta_{\mathrm{bm}}\omega + \frac{\omega_{\mathrm{c}}^4}{r^2}\frac{M_{\mathrm{tm}}}{M_{\mathrm{bm}}}\zeta_{\mathrm{tm}}\omega.
\end{aligned}$$

The expression above is positive since ω is positive. Note a singularity when $r = 0$ or $\omega = \sqrt{\omega_{\mathrm{tm}}^2 + \omega_{\mathrm{c}}^2}$, which is where θ changes its value from 0 to $-\pi$.

bioRxiv preprint doi: https://doi.org/10.1101/2023.02.24.529908; this version posted February 25, 2023. The copyright holder for this preprint (which was not certified by peer review) is the author/funder, who has granted bioRxiv a license to display the preprint in perpetuity. It is made available under aCC-BY-ND 4.0 International license.

$$r_1\cos\theta_1 - \frac{\omega_c^4}{r}\frac{M_{tm}}{M_{bm}}\cos\theta$$

$$= r_1\cos\left(-\operatorname{atan2}\left(\zeta_{bm}\omega, -\omega^2 + \omega_{bm}^2 + \omega_c^2\frac{M_{tm}}{M_{bm}}\right)\right)$$

$$-\frac{\omega_c^4}{r}\frac{M_{tm}}{M_{bm}}\cos\left(-\operatorname{atan2}(\zeta_{tm}\omega, -\omega^2 + \omega_{tm}^2 + \omega_c^2)\right)$$

$$= r_1\cos\left(\operatorname{atan2}\left(\zeta_{bm}\omega, -\omega^2 + \omega_{bm}^2 + \omega_c^2\frac{M_{tm}}{M_{bm}}\right)\right)$$

$$-\frac{\omega_c^4}{r}\frac{M_{tm}}{M_{bm}}\cos\left(\operatorname{atan2}(\zeta_{tm}\omega, -\omega^2 + \omega_{tm}^2 + \omega_c^2)\right)$$

$$= r_1\frac{-\omega^2 + \omega_{bm}^2 + \omega_c^2\frac{M_{tm}}{M_{bm}}}{r_1} - \frac{\omega_c^4}{r}\frac{M_{tm}}{M_{bm}}\frac{-\omega^2 + \omega_{tm}^2 + \omega_c^2}{r}$$

$$= -\omega^2 + \omega_{bm}^2 + \omega_c^2\frac{M_{tm}}{M_{bm}} - \frac{\omega_c^4}{r^2}\frac{M_{tm}}{M_{bm}}(-\omega^2 + \omega_{tm}^2 + \omega_c^2).$$

For the purpose of understanding of θ_2, we are interested in the intervals where the expression above is positive or negative intervals. On the positive ω semi-axis, there are three points, defining such intervals. Two of them coincide with the system resonances φ_1 and φ_2 (see the derivation of the normal modes in the simplified case, when dampers are neglected below, in the solution to question 2) and $\omega = \sqrt{\omega_{tm}^2 + \omega_c^2}$. The expression is positive at $\omega = 0$. With increasing ω, it changes its sign after the first resonance to negative, then becomes positive after $\omega = \sqrt{\omega_{tm}^2 + \omega_c^2}$ and negative again after the second resonance frequency. If neglecting small terms,

$$\theta_2 = \begin{cases} 0, & 0 < \omega < \varphi_1, \\ \pi, & \varphi_1 < \omega < \sqrt{\omega_{tm}^2 + \omega_c^2}, \\ 0, & \sqrt{\omega_{tm}^2 + \omega_c^2} < \omega < \varphi_2, \\ \pi, & \omega > \varphi_2. \end{cases} \quad \text{(S22)}$$

Therefore,

bioRxiv preprint doi: https://doi.org/10.1101/2023.02.24.529908; this version posted February 25, 2023. The copyright holder for this preprint (which was not certified by peer review) is the author/funder, who has granted bioRxiv a license to display the preprint in perpetuity. It is made available under aCC-BY-ND 4.0 International license.

$$\delta_{\mathrm{bm}} = \begin{cases} \frac{\pi}{2}, & 0 < \omega < \varphi_1, \\ \frac{3\pi}{2}, & \varphi_1 < \omega < \sqrt{\omega_{\mathrm{tm}}^2 + \omega_{\mathrm{c}}^2}, \\ \frac{\pi}{2}, & \sqrt{\omega_{\mathrm{tm}}^2 + \omega_{\mathrm{c}}^2} < \omega < \varphi_2, \\ \frac{3\pi}{2}, & \omega > \varphi_2. \end{cases} \quad \text{(S23)}$$

This result is fully replicated in numerical modelling, see Figure 3E, note that δ_{bm} has an opposite sign from the BM phase.

Finally, let us consider the difference $Z_{\mathrm{bm}} - Z_{\mathrm{tm}}$.

$$Z_{\mathrm{bm}} - Z_{\mathrm{tm}} = A_{\mathrm{bm}} e^{i(\omega t - \delta_{\mathrm{bm}})} - A_{\mathrm{tm}} e^{i(\omega t - \delta_{\mathrm{tm}})} = A_{\mathrm{bm}} e^{i(\omega t - \delta_{\mathrm{bm}})} \left(1 - \frac{\omega_{\mathrm{c}}^2}{r} e^{i\theta}\right).$$

The relative phase of the difference is $\Delta_{\mathrm{ph}} = \theta_3 - \delta_{\mathrm{bm}}$, where $r_3 e^{-i\theta_3} = 1 - \omega_{\mathrm{c}}^2 e^{i\theta}/r$. Imaginary part of the latter expression is $-\omega_{\mathrm{c}}^2 \sin\theta / r$. Recall that θ is small since it is proportional to $\zeta_{\mathrm{tm}}\omega/\omega_{\mathrm{c}}^2$. Therefore, θ_3 is close to 0 or π, if the real part is positive or negative, correspondingly.

$$\mathrm{Re}\left(1 - \frac{\omega_{\mathrm{c}}^2}{r} e^{i\theta}\right) = 1 - \frac{\omega_{\mathrm{c}}^2}{r}\cos\theta = 1 - \frac{\omega_{\mathrm{c}}^2}{r^2}(-\omega^2 + \omega_{\mathrm{tm}}^2 + \omega_{\mathrm{c}}^2).$$

Omitting the details of derivation, there are two points, which divide the positive ω semi-axis into three intervals. The first point is close to ω_{tm} and the second one is close to the singularity $\sqrt{\omega_{\mathrm{tm}}^2 + \omega_{\mathrm{c}}^2}$. The real part is positive in the first interval between 0 and ω_{tm}, then changes the sign to negative between ω_{tm} and $\sqrt{\omega_{\mathrm{tm}}^2 + \omega_{\mathrm{c}}^2}$, then changes the sign again to positive on $\omega > \sqrt{\omega_{\mathrm{tm}}^2 + \omega_{\mathrm{c}}^2}$. After combining everything together and if neglecting small terms, the phase of the difference takes the following values

$$\Delta_{\mathrm{ph}} = \theta_3 - \delta_{\mathrm{bm}} = \begin{cases} -\frac{\pi}{2}, & 0 < \omega < \omega_{\mathrm{tm}}, \\ \frac{\pi}{2}, & \omega_{\mathrm{tm}} < \omega < \varphi_1, \\ -\frac{\pi}{2}, & \varphi_1 < \omega < \varphi_2, \\ -\frac{3\pi}{2}, & \omega > \varphi_2 \end{cases} \quad \text{(S24)}$$

bioRxiv preprint doi: https://doi.org/10.1101/2023.02.24.529908; this version posted February 25, 2023. The copyright holder for this preprint (which was not certified by peer review) is the author/funder, who has granted bioRxiv a license to display the preprint in perpetuity. It is made available under aCC-BY-ND 4.0 International license.

Note that at $\omega = \sqrt{\omega_{\mathrm{tm}}^2 + \omega_{\mathrm{c}}^2}$, both δ_{bm} and θ_3 change their values by $-\pi$, thus this jump is cancelled out and the value of Δ_{ph} remains.

The amplitude of the difference is

$$|Z_{\mathrm{bm}} - Z_{\mathrm{tm}}| = A_{\mathrm{bm}} r_3 = \frac{P_{\mathrm{a}}}{M_{\mathrm{bm}}} \frac{r_3}{r_2} = \frac{P_{\mathrm{a}}}{M_{\mathrm{bm}}} \frac{r_3}{r_2}.$$

This expression has singularities, which correspond to resonance frequencies (see discussion above regarding θ_2). For the sake of the space, instead of substituting all terms in the above expression, we can focus on the expression for r_3.

$$r_3^2 = \left(1 - \frac{\omega_{\mathrm{c}}^2}{r}\cos\theta\right)^2 + \left(\frac{\omega_{\mathrm{c}}^2}{r}\sin\theta\right)^2 = \frac{1}{r^2}(\omega^4 + \omega^2(-2\omega_{\mathrm{tm}}^2 + \zeta_{\mathrm{tm}}^2) + \omega_{\mathrm{tm}}^4)$$

The above shows that since the damping coefficient $0 < \zeta_{\mathrm{tm}} \ll \omega_{\mathrm{tm}}$, the minimal value of the amplitude of the difference is when $\omega = \sqrt{\omega_{\mathrm{tm}}^2 - 0.5\zeta_{\mathrm{tm}}^2} \approx \omega_{\mathrm{tm}} - 0.25\zeta_{\mathrm{tm}}^2/\omega_{\mathrm{tm}} \approx \omega_{\mathrm{tm}}$, which corrects the previous finding. Note, that at this frequency, r_3^2 is of the same order of magnitude as $\zeta_{\mathrm{tm}}^2 \ll 1$.

Answer to question 1: Minimum of the relative displacement ΔX between the TM and BM always occurs at the TM resonance frequency ω_{tm} (see also Figure 10 in Nankali et al., 2020). Its frequency position does not depend on the properties of the driven oscillator, i.e. the BM/OoC. The ΔX minimum becomes more pronounced with decreasing the TM damping.

To answer question 2, let us consider the original system of equations (4, 5) without dampers and external force to find frequencies of the normal modes:

$$\frac{d^2 X_{\mathrm{bm}}}{dt^2} + \omega_{\mathrm{bm}}^2 X_{\mathrm{bm}} - \omega_{\mathrm{c}}^2 (X_{\mathrm{tm}} - X_{\mathrm{bm}}) \left(\frac{M_{\mathrm{tm}}}{M_{\mathrm{bm}}}\right) = 0, \tag{S25}$$

$$\frac{d^2 X_{\mathrm{tm}}}{dt^2} + \omega_{\mathrm{tm}}^2 X_{\mathrm{tm}} + \omega_{\mathrm{c}}^2 (X_{\mathrm{tm}} - X_{\mathrm{bm}}) = 0. \tag{S26}$$

We look for a solution in the form of a cosine function

$$\begin{pmatrix} X_{\mathrm{bm}} \\ X_{\mathrm{tm}} \end{pmatrix} = \begin{pmatrix} x_{\mathrm{bm}} \\ x_{\mathrm{tm}} \end{pmatrix} \cos(\varphi t), \tag{S27}$$

then after substituting (S27) into (S25) and (S26) and using matrix notations we have

bioRxiv preprint doi: https://doi.org/10.1101/2023.02.24.529908; this version posted February 25, 2023. The copyright holder for this preprint (which was not certified by peer review) is the author/funder, who has granted bioRxiv a license to display the preprint in perpetuity. It is made available under aCC-BY-ND 4.0 International license.

$$\begin{pmatrix}1 & 0\\ 0 & 1\end{pmatrix}\begin{pmatrix}x_{\mathrm{bm}}\\ x_{\mathrm{tm}}\end{pmatrix}(-\varphi^2)\cos(\varphi t)+\begin{pmatrix}\omega_{\mathrm{bm}}^2+\omega_{\mathrm{c}}^2\dfrac{M_{\mathrm{tm}}}{M_{\mathrm{bm}}} & -\omega_{\mathrm{c}}^2\dfrac{M_{\mathrm{tm}}}{M_{\mathrm{bm}}}\\ -\omega_{\mathrm{c}}^2 & \omega_{\mathrm{tm}}^2+\omega_{\mathrm{c}}^2\end{pmatrix}\begin{pmatrix}x_{\mathrm{bm}}\\ x_{\mathrm{tm}}\end{pmatrix}\cos(\varphi t)=0. \quad \text{(S28)}$$

Rearranging yields

$$\begin{pmatrix}\omega_{\mathrm{bm}}^2+\omega_{\mathrm{c}}^2\dfrac{M_{\mathrm{tm}}}{M_{\mathrm{bm}}}-\varphi^2 & -\omega_{\mathrm{c}}^2\dfrac{M_{\mathrm{tm}}}{M_{\mathrm{bm}}}\\ -\omega_{\mathrm{c}}^2 & \omega_{\mathrm{tm}}^2+\omega_{\mathrm{c}}^2-\varphi^2\end{pmatrix}\begin{pmatrix}x_{\mathrm{bm}}\\ x_{\mathrm{tm}}\end{pmatrix}\cos(\varphi t)=0. \quad \text{(S29)}$$

A trivial solution is $\begin{pmatrix}x_{\mathrm{bm}}\\ x_{\mathrm{tm}}\end{pmatrix}=\begin{pmatrix}0\\ 0\end{pmatrix}$. To find non-trivial solutions the determinant of the matrix should be equal to zero, which leads to the following equation with respect to φ:

$$\begin{aligned}&\det\begin{pmatrix}\omega_{\mathrm{bm}}^2+\omega_{\mathrm{c}}^2\dfrac{M_{\mathrm{tm}}}{M_{\mathrm{bm}}}-\varphi^2 & -\omega_{\mathrm{c}}^2\dfrac{M_{\mathrm{tm}}}{M_{\mathrm{bm}}}\\ -\omega_{\mathrm{c}}^2 & \omega_{\mathrm{tm}}^2+\omega_{\mathrm{c}}^2-\varphi^2\end{pmatrix}\\ &=\left(\omega_{\mathrm{bm}}^2+\omega_{\mathrm{c}}^2\frac{M_{\mathrm{tm}}}{M_{\mathrm{bm}}}-\varphi^2\right)(\omega_{\mathrm{tm}}^2+\omega_{\mathrm{c}}^2-\varphi^2)-\omega_{\mathrm{c}}^4\frac{M_{\mathrm{tm}}}{M_{\mathrm{bm}}}=0. \quad \text{(S30)}\end{aligned}$$

After collecting coefficients of the powers of φ, we have

$$\varphi^4-\left(\omega_{\mathrm{bm}}^2+\omega_{\mathrm{tm}}^2+\omega_{\mathrm{c}}^2\left(\frac{M_{\mathrm{tm}}}{M_{\mathrm{bm}}}+1\right)\right)\varphi^2+\omega_{\mathrm{bm}}^2\omega_{\mathrm{tm}}^2+\omega_{\mathrm{c}}^2\left(\omega_{\mathrm{bm}}^2+\omega_{\mathrm{tm}}^2\frac{M_{\mathrm{tm}}}{M_{\mathrm{bm}}}\right)=0. \quad \text{(S31)}$$

After substituting $\Phi=\varphi^2$, the equation (S31) is reduced to a quadratic equation

$$\Phi_{1,2}=\frac{1}{2}\left(\left(\omega_{\mathrm{bm}}^2+\omega_{\mathrm{tm}}^2+\omega_{\mathrm{c}}^2\left(\frac{M_{\mathrm{tm}}}{M_{\mathrm{bm}}}+1\right)\right)\pm\sqrt{\left(\omega_{\mathrm{bm}}^2-\omega_{\mathrm{tm}}^2\right)^2+\omega_{\mathrm{c}}^4\left(\frac{M_{\mathrm{tm}}}{M_{\mathrm{bm}}}+1\right)^2+2\omega_{\mathrm{c}}^2\left(\frac{M_{\mathrm{tm}}}{M_{\mathrm{bm}}}-1\right)\left(\omega_{\mathrm{bm}}^2-\omega_{\mathrm{tm}}^2\right)}\right). \quad \text{(S32)}$$

Note that both Φ_1 and Φ_2 are positive and we can find frequencies of the normal modes $\varphi_{1,2}=\sqrt{\Phi_{1,2}}$. For the chosen model parameters $\varphi_1=1.37$ and $\varphi_2=5.35$.

Answer to question 2: The second normal mode of the system is shifted towards high frequencies due to strong coupling K_{c} between the TM and OoC, and its contribution for frequencies below ω_{bm} is minimal.

Answer to question 3: The local minimum of ΔX is always observed at ω_{tm} (see answer to question 1). Therefore, it is not observed when $K_{\mathrm{tm}}=0$, the TM limbal attachment is absent and $\omega_{\mathrm{tm}}=0$. Two normal modes of the system (equation (S32)) exist.